Slit/Robo Signaling Modulates the Proliferation of Central Nervous System Progenitors

Víctor Borrell[1],[*], **Adrián Cárdenas**[1], **Gabriele Ciceri**[1], **Joan Galcerán**[1], **Nuria Flames**[1], **Ramón Pla**[1], **Sandrina Nóbrega-Pereira**[1], **Cristina García-Frigola**[1], **Sandra Peregrín**[1], **Zhen Zhao**[2], **Le Ma**[2], **Marc Tessier-Lavigne**[3], and **Oscar Marín**[1],[*]

[1]Instituto de Neurociencias, Consejo Superior de Investigaciones Científicas & Universidad Miguel Hernández, Sant Joan d'Alacant 03550, Spain

[2]Department of Cell and Neurobiology, Zilkha Neurogenetic Institute, Keck School of Medicine, University of Southern California, Los Angeles, CA 90033, USA

[3]Laboratory of Brain Development and Repair, Rockefeller University, 1230 York Avenue, New York, NY 10065, USA

SUMMARY

Neurogenesis relies on a delicate balance between progenitor maintenance and neuronal production. Progenitors divide symmetrically to increase the pool of dividing cells. Subsequently, they divide asymmetrically to self-renew and produce new neurons or, in some brain regions, intermediate progenitor cells (IPCs). Here we report that central nervous system progenitors express Robo1 and Robo2, receptors for Slit proteins that regulate axon guidance, and that absence of these receptors or their ligands leads to loss of ventricular mitoses. Conversely, production of IPCs is enhanced in *Robo1/2* and *Slit1/2* mutants, suggesting that Slit/Robo signaling modulates the transition between primary and intermediate progenitors. Unexpectedly, these defects do not lead to transient overproduction of neurons, probably because supernumerary IPCs fail to detach from the ventricular lining and cycle very slowly. At the molecular level, the role of Slit/Robo in progenitor cells involves transcriptional activation of the Notch effector *Hes1*. These findings demonstrate that Robo signaling modulates progenitor cell dynamics in the developing brain.

INTRODUCTION

Robo receptors are important regulators of axon guidance and cell migration in vertebrates and invertebrates (Brose et al., 1999; Dickson and Gilestro, 2006; Legg et al., 2008). In response to Slit proteins, Robo signaling influences the cytoskeleton to promote repulsion, attraction, or branching, depending on the cellular context (Kidd et al., 1998; Kramer et al.,

2001; Long et al., 2004; Wang et al., 1999; Whitford et al., 2002), which allows for a great diversity of biological functions. Using similar mechanisms, Slit/Robo signaling also regulates a large variety of morphogenetic processes outside the central nervous system (CNS), from leukocyte chemotaxis and angiogenesis to kidney and cardiac development (Fish et al., 2011; Grieshammer et al., 2004; Kramer et al., 2001; Legg et al., 2008; London and Li, 2011; Ypsilanti et al., 2010).

Three of the four Robo receptors that are encoded in the mammalian genome are expressed in the CNS, with *Robo1* and *Robo2* displaying the most widespread patterns in the developing brain (Marillat et al., 2001). Slits are the principal ligands for the Robo receptors (Kidd et al., 1999), to which they bind in association with heparan sulfate proteoglycans (Hu, 2001). There are three *Slit* genes in mammals, and all of them are expressed in developing CNS (Marillat et al., 2001). Slits bind promiscuously to Robo receptors in vitro (Brose et al., 1999; Li et al., 1999), which suggests that these proteins may cooperate in vivo in those locations in which their expression patterns overlap (Bagri et al., 2002; Plump et al., 2002).

The functions of Robo receptors have been classically studied in postmitotic cells, most typically in neurons. However, Robo receptors also seem to be expressed in progenitor cells, at least in some regions of the developing brain (Marillat et al., 2001). A few studies have even hinted at a possible role for Robo receptors in neurogenesis (Andrews et al., 2008; Mehta and Bhat, 2001), but the precise mechanisms through which Slit signaling may control this process are unknown. In *Drosophila*, slit seems to modulate neurogenesis by promoting asymmetric terminal divisions in particular neural lineages (Mehta and Bhat, 2001). Considering the highly conserved roles of Slits and their Robo receptors in evolution (Brose and Tessier-Lavigne, 2000), it is conceivable that Slit/Robo signaling may play a similar role in the vertebrate brain.

Here we have tested the hypothesis that Slit/Robo signaling may contribute to regulate neurogenesis in the mammalian CNS. We focused most of our analysis in the developing cerebral cortex, for which the cellular mechanisms of neurogenesis are beginning to be elucidated (Fietz and Huttner, 2011; Noctor et al., 2007; Pontious et al., 2008). During early phases of neurogenesis, cortical progenitor cells residing in the ventricular zone (VZ) divide symmetrically to increase the pool of dividing cells. As neurogenesis progresses, VZ progenitors begin to divide asymmetrically to self-renew and produce new neurons or, more frequently, to generate IPCs. These progenitors, which localize to the subventricular zone (SVZ), will generate additional neurons after one or more rounds of divisions. This two-step process of neurogenesis is highly reminiscent to that observed during the development of the CNS in *Drosophila* (Skeath and Thor, 2003), but the mechanisms controlling these dynamics remain poorly characterized.

We found that progenitor cells throughout the entire mouse brain and spinal cord transiently express Robo1 and Robo2, in particular during early stages of neurogenesis. Analysis of *Robo1* and *Robo2* double (*Robo1/2*) mutants revealed that these receptors are required to maintain the proper balance between primary and intermediate progenitors, because loss of Robo signaling leads to a decrease in VZ progenitors and a concomitant increase in the

number of IPCs. Slit proteins likely mediate this function, because similar defects were found in *Slit1* and *Slit2* double (*Slit1/2*) mutants. We found that Robo receptors maintain cortical progenitor balance through interaction with the Notch pathway by controlling *Hes1* transcription. Our study uncovers a novel role for Slit/Robo signaling in progenitor cells, which expands the vast repertoire of biological functions already attributed to this highly conserved pathway.

RESULTS

Reduced Volume and Thickness of the Cortex in Robo1/2 Mutants

We have previously reported that *Robo1/2* mutants are essential for the development of major axonal projections in the mouse-developing forebrain (López-Bendito et al., 2007). As part of this analysis, we found that the brain of *Robo1/2* mutants is smaller than controls at birth (Figure 1A). For example, the volume of the telencephalon and thalamus in *Robo1/2* mutants was consistently smaller than controls as early as E14.5 (Figures 1C–1G; data not shown). The thickness of the neocortex was also significantly reduced in *Robo1/2* mutants compared to controls (Figures 1D, 1F, and 1G). Despite this difference, layer formation in the developing cortex seems to proceed normally (Figures 1B and S1 available online). We reasoned that the prominent axon guidance defects that exist in *Robo1/2* mutants could explain part of the size differences observed in our analyses (López-Bendito et al., 2007). However, we also noticed that the cortical germinal epithelium of *Robo1/2* mutants was much thinner than that of control brains at birth (red brackets in Figures 1B, 1D, and 1F). Since these defects could not be simply explained by defective axons, this finding prompted us to study a possible role of Robo signaling in neural progenitors.

Impaired Neurogenesis Dynamics in *Robo1/2* Mutants

To assess a possible role for Robo receptors in neural precursor cells, we first examined the expression of *Robo1* and *Robo2* messenger RNA (mRNA) in progenitor regions throughout the developing CNS. We found that *Robo1* and *Robo2* are expressed in most progenitor epithelia in the developing forebrain (E12.5) and spinal cord (E9.5) (red asterisks in Figures 2A–2F), although different regions predominantly express one of the receptors. For example, progenitor cells in the VZ of the developing pallium express relatively high *Robo2* mRNA levels (Figures 2C, 2D, and S2A–S2J), while *Robo1* is more abundantly expressed in the VZ of the medial and lateral ganglionic eminences (MGE and LGE, respectively; Figures 2C, 2D, and S2A–S2J). Consistently, immunohistochemical experiments revealed expression of Robo2 in the VZ of the cortex with barely detectable levels of Robo1 (Figures 2G and 2J). Nevertheless, semiquantitative RT-PCR and western blot analyses in tissue obtained from the cortex of E10.5 embryos revealed expression of both receptors (Figures S2K and S2L). These results confirmed the presence of Robo1 and Robo2 in progenitor cells, because the mouse cerebral cortex is almost entirely devoid of neurons at this early stage.

We also discovered that the expression of Robo receptors in progenitor regions followed a very dynamic pattern. For instance, *Robo1* and *Robo2* were found in the VZ of the developing telencephalon as early as E10.5, but their expression declined with age and was

almost absent, except for discrete sites, after E14.5 (Figures S2A–S2J). This temporal course of expression in progenitor cells suggested that Robo receptors might primarily influence dividing cells at early stages of neurogenesis.

To directly test this hypothesis, we examined the density of dividing cells (number of mitotic cells per length of VZ) in different regions of the CNS in control and *Robo1/2* mutants. We found that the density of progenitor cells in mitosis, as revealed with the M-phase marker phospho-Histone H3 (PH3), was consistently reduced in all regions examined, including the spinal cord, thalamus, MGE and LGE, and cortex (Figures 2H, 2I, 2K, and S3). Thus, Robo1 and Robo2 receptors are expressed in progenitor cells throughout the CNS, and their simultaneous deletion leads to a decrease in the density of dividing VZ cells during early stages of neurogenesis.

To analyze the basis of this phenotype, we focused our analysis in the developing neocortex. We reasoned that a smaller density of mitoses in the VZ of the cortex could impact on the rate of VZ progenitor self-renewal, thus leading to reduced numbers of VZ progenitor cells and, consequently, to a less extensive VZ. Consistent with this prediction, we found that the length of the cortical VZ was significantly smaller in E11.5 and E12.5 *Robo1/2* mutant embryos compared to controls (Figures 2L–2N). One possible explanation for the reduced density of mitoses could be that loss of *Robo1/2* leads to increased cell death in VZ progenitors. However, quantification of the density of apoptotic cells (identified by expression of cleaved Caspase 3) revealed no differences between control and *Robo1/2* mutants (control: 6.2 ± 0.7 cells/mm, n = 4; mutant: 7.6 ± 0.8 cells/mm; n = 4, mean $\pm$ SEM, p = 0.23). Thus, the reduced length of ventricular lining observed in *Robo1/2* mutants does not seem to arise as a consequence of enhanced cell death.

The decreased density of VZ mitoses found in *Robo1/2* mutants at these early stages of neurogenesis could also be caused by a shift in the type of division occurring at the VZ, from symmetric to asymmetric. In other words, instead of expanding the pool of dividing cells, VZ cells might have a higher tendency to prematurely produce neurons or IPCs in *Robo1/2* mutants. To test this idea, we analyzed the thickness of the postmitotic neuronal layer using neuron-specific antibodies against β-III-Tubulin, TuJ1. We found no significant differences between control and *Robo1/2* mutants (control: 33.5 ± 2.0 μm, n = 12; mutant: 30.4 ± 2.0 μm; n = 15, mean $\pm$ SEM, p = 0.29) (Figures 3C and 3D), thus suggesting no changes in neuron production at E12.5. In contrast, quantification of the number of IPCs, as revealed by the expression of the T-box transcription factor Tbr2 (Pontious et al., 2008), showed that the cortex of *Robo1/2* mutants contains almost twice as many Tbr2+ cells as controls at E12.5 (Figures 3A–3E). Because Tbr2 may also label some differentiating neurons (Pontious et al., 2008), we next analyzed the fraction of these cells that also expressed the proliferation marker Ki67. We observed that the number of Tbr2+ progenitor cells (IPCs) in the cortex of *Robo1/2* mutants was almost double than in controls at E12.5 (Figures 3F–3H). Thus loss of Robo1/2 function leads to a depletion of VZ progenitors and to an abnormal increase in the numbers of IPCs in the developing cerebral cortex. Analysis of *Robo1* and *Robo2* single mutant embryos revealed that the phenotypic changes found in the cortex of *Robo1/2* mutants were primarily due to the loss of *Robo2* (Figure S4). Nevertheless, the raise in the number of IPCs found in *Robo2* single mutants is milder than

in *Robo1/2* double mutants, which suggested that Robo1 cooperates with Robo2 in regulating the production of IPCs. Altogether, these results indicated that Robo receptors modulate neurogenesis in the developing brain.

Slits Mediate the Effects of Robo Receptors in Neurogenesis

Slit proteins are the ligands of Robo receptors in cell guidance, and so we tested whether Slits also mediate the function of Robo receptors in neurogenesis. Analysis of the distribution of *Slit1* and *Slit2* mRNA at different developmental stages revealed multiple sources of Slit proteins that could influence telencephalic progenitor cells (Figures 4A, 4B, and S5A–S5J). We were particularly intrigued by the expression of Slits in the choroid plexus and in other cells lining the ventricle, because recent work suggests that factors present in the cerebrospinal fluid (CSF) modulate the proliferation of cortical progenitor cells (Lehtinen et al., 2011). Consistent with this idea, we found that Slit proteins are indeed present in the CSF of mouse embryos at E12.5 (Figure 4C). We also observed that a recombinant Slit2-alkaline phosphatase fusion protein (Slit2-AP) binds homogenously throughout the ventricular surface of E12.5 telencephalic hemispheres (Figure 4D). This experiment reinforced the idea that Slits present in the CSF may bind to Robo receptors expressed by progenitor cells in contact with the ventricle, thereby modulating neurogenesis at early stages of cortical development.

To directly test the function of Slits in regulating the proliferation of cortical progenitors, we analyzed progenitor cell dynamics in *Slit* mutants. Analysis of *Slit1* and *Slit2* single mutant embryos revealed no differences in the density of PH3+ VZ progenitor cells or in the number of Tbr2+ IPCs (Figures S5K–S5R). In contrast, we found that the density of PH3+ nuclei in the VZ of the developing cortex was reduced in *Slit1/2* double mutants compared to controls (Figures 4E, 4F, and 4I). In addition, we observed that the amount of Tbr2+ cells was greatly increased in *Slit1/2* double mutants compared to controls (Figures 4G–4I). These results demonstrate that simultaneous loss of Slit1 and Slit2 causes a similar phenotype to that found in *Robo1/2* mutants, which reinforces the view that Slit/Robo signaling modulates early neurogenesis.

Deficient Cell Cycle Progression in *Robo1/2* Mutants

IPCs may divide symmetrically to generate two new IPCs, but most frequently they produce a pair of newborn neurons (Haubensak et al., 2004; Huttner and Kosodo, 2005; Noctor et al., 2004). However, neurogenesis did not seem to increase in *Robo1/2* and *Slit1/2* mutants, despite the prominent expansion in the pool of IPCs (Figures 3C, 3D, 4H, and 4I). This suggested that IPCs fail to produce a normal complement of neurons in the absence of Slit/ Robo signaling. Consistent with this view, analysis of the fraction of cells leaving the mitotic cycle (quitting fraction) revealed a prominent decrease in *Robo1/2* mutants compared to controls (Figures 3I–3K). Furthermore, although IPCs are more abundant in the cortex of *Robo1/2* mutants than controls, quantification of the number of mitoses in basal (SVZ) positions revealed no differences between control and *Robo1/2* mutants (Figures 2H, 2I, and 2K). Together, these experiments suggested that IPCs divide less frequently in *Robo1/2* mutants. To confirm this hypothesis, we measured the length of the cell cycle of IPCs. We found that cell cycle length is significantly longer in *Robo1/2* mutants than in

controls (control Tc: 11.5 hr; mutant Tc: 14.6 hr) (Figure S6A), while no differences where observed in the process of interkinetic nuclear migration (Figures S6B–S6H). In sum, loss of Robo1/2 signaling causes an overproduction of IPCs in the cerebral cortex, but this defect does not lead to enhanced neurogenesis, because they divide at a slow rate.

Robo Function in Neurogenesis Is Cell Autonomous

To gain further insight into the cellular mechanisms underlying these defects, we next performed a clonal analysis of progenitor cells in the cerebral cortex of control and *Robo1/2* mutants. Using ultrasound-guided imaging, we made intraventricular injections of low-titer green fluorescent protein (*Gfp*)-expressing retrovirus at E11.5 to mark individual cortical progenitor cells and analyzed their clonal progeny at E13.5 (Figures 5A–5E and S7A–S7E′). First, we found that large clones were relatively more abundant in *Robo1/2* mutants than in controls (Figure S7F), consistent with our previous observation that cell cycle exit is reduced in the cortex of *Robo1/2* mutants (Figures 3I–3K). Despite this variation in clone size, the number of postmitotic TuJ1+ neurons per clone did not differ between controls and mutants (Figures 5B–5E, 5H, and S7G), which suggested that individual clones in *Robo1/2* mutants contain more progenitors than in controls. Consistent with this idea, we observed that Tbr2+ cells were more abundant in individual clones from *Robo1/2* mutants than in controls (Figure 5H).

We next examined whether Robo1/2 signaling influences progenitor dynamics in a cell-autonomous manner. To this end, we performed a new series of clonal tracing experiments in wild-type embryos using retroviruses encoding *Gfp* and a dominant negative variant of *Robo2* (*DN-Robo2*, Figure 6A) (Stein and Tessier-Lavigne, 2001). Analysis of individual clones derived from cortical progenitor cells revealed that expression of *DN-Robo2* causes very similar defects to those observed in *Robo1/2* mutants. For example, Tbr2+ cells were more abundant in individual clones expressing *DN-Robo2* than in controls, whereas the total number of postmitotic TuJ1+ cells remained unchanged (Figures 6B–6F). In reciprocal experiments, we used in utero electroporation to overexpress a plasmid encoding a myristoylated form of the cytoplasmic domain of *Robo2* (*mR2*), which acts as a constitutively active form of the receptor (Figure 6G) (Bai et al., 2011). Consistent with our previous results, we observed that increased Robo signaling significantly reduces the fraction of Tbr2+ cells among the electroporated cells (Figures 6H–6J). Altogether, these gain and loss of function experiments demonstrated that Robo receptors modulate progenitor cell dynamics in a cell-autonomous manner.

Robo Function Is Required for the Detachment of Intermediate Progenitors

The clonal analysis of progenitor cells in the cerebral cortex also revealed that *Robo1/2* mutant clones (Figures 5B–5E, 5H, and S7H) and *DN-Robo2*-expressing clones (Figures 6B–6F) contained many more progenitor cells with an apical process than control clones. This finding was unexpected, since progenitor cells with an apical process have been typically described as VZ progenitors (Noctor et al., 2002), and our previous observa tions suggested that *Robo1/2* mutants contain fewer VZ progenitors than controls (Figure 2). Interestingly, we found that a small percentage of Tbr2+ IPCs display an apical process in control clones (~6%) (Figures 5F–5F″ and 5H), perhaps reflecting that IPCs maintain

contact with the ventricle for several hours after being generated (Noctor et al., 2008). Remarkably, the percentage of Tbr2+ IPCs that display an apical process was greatly increased in *Robo1/2* mutant clones (~15%) (Figures 5G and 5H) and in *DN-Robo2-*expressing clones (~20%) (Figures 6B–6F). Conversely, the fraction of Tbr2+ IPCs that display an apical process was significantly decreased in *mR2*-expressing clones (Figures 6H–6J). This analysis suggested that Robo signaling not only influences the generation of IPCs, but also their separation from the ventricular surface. In agreement with this idea, we found that the fraction of Tbr2+ cells containing low levels of Pax6, which presumably identifies nascent IPCs (Arai et al., 2011), is increased in *Robo1/2* mutants (Figures 3L–3N). These results reinforced the view that the supernumerary IPCs generated in *Robo1/2* mutants are stuck in their progression away from the VZ. Since the detachment of IPCs has been shown to influence their proliferation (Cappello et al., 2006), this defect may explain why the enhanced production of IPCs in *Robo1/2* mutants does not lead to increased neurogenesis.

Robo Signaling Is Required for Normal *Hes1* Levels in Progenitor Cells

Our previous experiments suggested that the abnormal progression of IPCs in *Robo1/2* mutants is likely due to increased adhesion. However, the existence of proliferation defects in the cortex of *Robo1/2* mutants as early as E10.5 suggested that Robo signaling might influence neurogenesis in a more direct manner. To test this hypothesis, we examined the status of three of the main signaling pathways controlling cortical neurogenesis, Notch, fibroblast growth factor (FGF), and WNT, by analyzing the expression of their effector genes *Hes1*, *Spry2*, and *Axin2*, respectively. Using quantitative PCR (qPCR), we found that the expression of basic helix-loop-helix (bHLH) gene *Hes1* was significantly reduced in the cortex of E12.5 *Robo1/2* mutants compared to controls (Figure 7A). In contrast, no significant changes were observed in mRNA levels for *Spry2* and *Axin2* (Figure S8A). Thus loss of Robo signaling seems to disrupt the expression of the Notch signaling effector *Hes1* in the absence of generalized changes in other important signaling pathways that are known to be active in progenitor cells.

We next examined the expression of several other components of the Notch signaling pathway. We found no significant changes in total mRNA levels for the Notch ligand *Dll1*, *Notch1*, or *Hes5*, another target gene of Notch signaling (Figure 7A; data not shown). mRNA analysis by in situ hybridization confirmed the reduction of *Hes1* in progenitor cells of the cerebral cortex (Figures 7B and S8B). In addition, it revealed that expression of *Dll1*, which is negatively regulated by *Hes1*, was increased in scattered cells throughout the VZ of the *Robo1/2* mutant cortex compared to controls (Figures 7B and S8B).

A reduction in *Hes1* levels could explain the decreased number of VZ mitosis and the increase in IPCs found in the *Robo1/2* mutant cortex, because *Hes1* expression is thought to maintain the status of progenitor cells in the VZ (Ishibashi et al., 1994; Nakamura et al., 2000). To experimentally test this hypothesis, we first attempted to rescue the IPC phenotype observed in *Robo1/2* mutants by overexpressing *Hes1*. To this end, we electroporated a plasmid encoding *Gfp*, alone or in combination with full length *Hes1*, in the cortex of *Robo1/2* mutant embryos at E12.5 and analyzed the expression of Tbr2 in

electroporated cells 24 hr later (Figure 7C). We found that overexpression of *Hes1* in *Robo1/2* mutant progenitor cells dramatically reduced the fraction of Tbr2+ cells within the electroporated clones (Figures 7D–7F). In reciprocal experiments, we knocked down Hes1 protein levels by using RNA interference. In brief, we electroporated chemically synthesized small interference RNA (siRNA) that has been previously shown to produce significant knockdown of mouse *Hes1* (Noda et al., 2011; Ross et al., 2004) or control siRNA, along with a plasmid encoding *Gfp*, in the cortex of wild-type embryos at E12.5 and analyzed the expression of Tbr2 in electroporated cells 48 hr later (Figure 7G). We observed that reducing *Hes1* levels in cortical progenitor cells increases the proportion of Tbr2+ cells within the electroporated clones (Figures 7H–7J). Altogether, these experiments supported the view that Robo receptors modulate progenitor dynamics at least in part through the regulation of *Hes1*.

Robo Signaling Regulates *Hes1* and Acts Synergistically to Notch

We next tested whether Robo signaling might directly enhance transcription of *Hes1* in VZ progenitor cells. To test this hypothesis, we performed luciferase activity assays in E12.5 primary cortical cultures containing a majority of cortical progenitor cells. In control experiments, we cotransfected cortical cells with a luciferase reporter construct containing a basic *Hes1* promoter (*Hes-Luc*) and a plasmid encoding the intracellular domain of Notch (*NICD*). We observed that NICD expression in cortical cells resulted in three-fold increase in luciferase activity over basal levels (Figure 8A). In parallel experiments, we found that cotransfection of the *Hes-Luc* reporter along with *mR2* also led to a significant increase in luciferase activity (Figure 8A). This effect was not observed in experiments in which we expressed a nonspecific myristoylated protein (mCFP, data not shown), suggesting that the effect observed for *mR2* was specific. These experiments strongly suggested that Robo signaling enhances *Hes1* transcription in cortical cells.

To test whether Robo-mediated *Hes1* transcription was dependent on Notch signaling, we performed similar experiments using a line of mouse neuroblastoma cells (Neuro-2a) that has been reported to lack Notch signaling (Franklin et al., 1999). We first verified that Notch signaling is not induced in Neuro-2a cells by transfecting these with a Notch reporter construct (*Nrep*) containing four RBP-J repeats (Figure 8B). We found that Neuro-2a cells fail to activate *Nrep* in the absence of exogenous Notch, even when they were cultured in the presence of Dll1-expressing cells or *mR2* (Figure 8B). However, we observed that cotransfection of Neuro-2a with Notch was sufficient to activate *Nrep*, even in the absence of Dll1-expressing cells (Figure 8B). These experiments confirmed that Neuro-2a cells lack Notch, but they seem to express Notch ligands and have the proper intracellular machinery to activate this pathway.

We next used Neuro-2a cells to test whether Robo signaling can activate *Hes1* transcription in the absence of Notch. To this end, we cotransfected Neuro-2a cells with the basic *Hes-Luc* reporter or with another plasmid containing a longer region of the *Hes1* promoter (2.6 *Hes-Luc*). We found that Robo activation led to increased transcriptional activity from both reporters, more prominently with the long *Hes1* promoter (Figure 8C). These results indicate that Robo signaling can activate *Hes1* independently of Notch signaling. To test a possible

cooperative effect of both signaling systems on *Hes1* transcription, we next cotransfected Neuro-2a cells with both *NICD* and *mR2*, together with the 2.6 *Hes-Luc* reporter. We found that Robo activation doubled the activity of *NICD* alone (Figure 8C), which demonstrates that Robo and Notch can function synergistically.

Finally, we dissected the contribution of different signaling modules of the Robo2 receptor to its transcriptional activity. Robo receptors have a long cytoplasmic tail that contains four blocks of conserved cytoplasmic (CC) sequences (Bashaw et al., 2000; Kidd et al., 1998). We performed luciferase activity assays in Neuro-2a cells using different constructs encoding truncated forms of mR2 (Figure 8D). Removal of CC3 from *Robo2* (*mR2 D1*) did not alter the activation of the luciferase reporter (Figure 8D), suggesting that Robo-mediated transcriptional activation of *Hes1* is independent of the Abelson tyrosine kinase (*Abl*), which binds this domain (Bashaw et al., 2000). In contrast, induction of luciferase transcription was severely impaired in the absence of CC2 and CC3 (*mR2 D2*; Figure 8D) and was completely absent when Robo receptors lacked CC1 to CC3 (*mR2 D3*; Figure 8D). These experiments demonstrate that several domains within the intracellular region of Robo receptors are required for their function on gene regulation.

DISCUSSION

Our results provide evidence that Slit/Robo signaling modulates progenitor dynamics during CNS development (Figure 9). This is an unexpected finding for a classical guidance receptor, thereby expanding the range of biological functions previously attributed to this signaling pathway (Legg et al., 2008; Ypsilanti et al., 2010). Robo receptors modulate neurogenesis at least in part through an interaction with the Notch pathway that involves the transcriptional control of *Hes1*, a previously unanticipated target of Robo signaling. Our results support previous studies suggesting that Slit signaling influences the pattern of cell division in *Drosophila* (Mehta and Bhat, 2001) and indicate that this function might be conserved during evolution. Thus Robo receptors may have evolved as pleio- tropic proteins that can control very different functions, depending on the cellular context.

Robo Signaling in Progenitor Cells

The function of Slit/Robo signaling in the CNS has been classically examined in postmitotic neurons, in which expression of Robo receptors is very prominent (Marillat et al., 2001). We found, however, that progenitor cells throughout the CNS also express Robo1 and Robo2 at early stages of neurogenesis, which prompted us to examine their possible function. Our analysis suggests that Slit/Robo signaling influences neurogenesis by favoring the self-renewal of VZ progenitors, at least during the initial phases of neurogenesis. In the cerebral cortex, VZ progenitors begin to produce an excess of IPCs in the absence of Slits or Robo receptors causes, which leads to an expansion of the pool of secondary progenitor cells. Our clonal experiments indicate that these defects are cell-autonomous, but future studies using conditional alleles for *Robo1* and *Robo2* should be performed to rule out any possible contribution of systemic defects to this phenotype.

An interesting aspect of this phenotype is that the excessive number of IPCs does not lead to enhanced neuronal production, as it would have been expected based on the analysis of mice

in which defective signaling in the VZ causes an overproduction of IPCs (Cappello et al., 2006). Instead, IPCs in *Robo1/2* mutants divide much slower than normal, which eventually leads to a relatively normal rate of neuronal production. It is conceivable that this phenotype might be secondary to the failure of IPCs to retract their apical process from the VZ. Indeed, an exploratory analysis of the organization of adherens junctions in *Robo1/2* mutants revealed abnormal levels of some proteins, most prominently N-Cadherin (Figure S9). This idea is consistent with previous results demonstrating that Robo signaling inhibits cadherin-based adhesions in other cellular contexts (Rhee et al., 2002; Wong et al., 2012; Zhou et al., 2011).

Our results are in sharp contrast with previous work suggesting that loss of Slit/Robo signaling leads to an increase in the number of mitosis in the VZ of the subpallium (Andrews et al., 2008). Other than possible differences in strain backgrounds or methodological considerations, we cannot explain the origin of this discrepancy. Our analysis reveals small but consistent deficits in VZ mitosis throughout the CNS, indicating that this phenotype is not restricted to a particular brain region. Based on the increased number of IPCs in *Robo* mutants, we interpreted the reduced number of VZ mitosis as a premature shift from symmetric to asymmetric cell divisions. This would suggest that Slit/Robo signaling might be mostly involved in controlling the mode of cell division in neural progenitors and not so much their rate. This interpretation is consistent with previous work in *Drosophila*, in which loss of Slit has been shown to modify the pattern of cell division for specific neural lineages (Mehta and Bhat, 2001). It is also worth mentioning that *Robo2* levels have been reported to decrease in the cortex of E13.5 mouse mutants for *insulinoma-associated 1*, a panneurogenic gene that regulates the balance between apical and basal progenitors in the developing cortex (Farkas et al., 2008). This process also seems regulated by FGF signaling, because *Fgfr1/2/3* triple mutant mice also exhibited a loss of apical progenitors and an increase of Tbr2+ basal progenitors (Kang et al., 2009).

Although Robo signaling has been classically linked to the cytoskeleton (Bashaw et al., 2000; Hu et al., 2005; Rhee et al., 2002; Wong et al., 2001; Yang and Bashaw, 2006), the unexpected function of Robo receptors in neural progenitor cells prompted us to explore alternative signaling pathways. Intriguingly, Robo function in progenitor cells appears to be mediated, at least in part, by transcriptional regulation. Previous studies have proposed that Robo signaling might modulate transcription in other cellular contexts (Grieshammer et al., 2004; Rhee et al., 2007), although no direct targets were identified. Our findings identify the bHLH gene *Hes1* as a likely target of Slit/Robo signaling and suggest that specific cytoplasmic modules in Robo receptors are required for this activity. Robo signaling promotes *Hes1* transcription in a manner that is independent of and synergistic to Notch signaling, indicating that these pathways cooperate during neural proliferation, as it has been suggested in other contexts (Redmond et al., 2000; Whitford et al., 2002). In the cerebral cortex, reduction in the levels of *Hes1* in VZ progenitors (paralleled by upregulation of *Dll1* in scattered cells) perturbs the balance between the symmetric expansion of primary progenitors and the asymmetric generation of IPCs in favor of this second pathway (Hansen et al., 2010; Kawaguchi et al., 2008; Mizutani et al., 2007; this study). In this context, our results support the idea that *Dll1* activation may not inexorably lead to neurogenesis, but,

depending on the cellular environment, it may also lead to the generation of IPCs (Hämmerle and Tejedor, 2007). Consistently, we found that proneural gene expression is moderately reduced throughout the developing forebrain of *Robo1/2* mutants (Figures S8C and S8D). In sum, our results demonstrate that Robo signaling cooperates with Notch, at least in part, through the regulation of *Hes1* RNA levels. The mechanisms through which this process occurs remain to be elucidated, although our experiments suggest that Robo signaling does not directly interfere with RBP-J binding sites.

Guidance Receptors and Progenitor Dynamics

The idea that a classical guidance receptor can also control cell division is not entirely new, since several recent studies have shown that other guidance molecules may influence progenitor cells in a number of different biological contexts. In particular, there is increasing evidence suggesting that Eph/ephrin signaling regulates proliferation in stem cells, both in the adult brain and in several other organs (Chumley et al., 2007; Conover et al., 2000; Genander and Frisén, 2010; Holmberg et al., 2005). In addition, Eph/ephrin signaling has been directly involved in controlling progenitor dynamics in the developing cortex. For instance, ephrin-A regulates the rate of apoptosis in cortical progenitor cells (Depaepe et al., 2005), whereas loss of ephrin-B1 causes an early depletion of VZ progenitor cells in the developing cortex (Qiu et al., 2008), a phenotype that is reminiscent to that observed for *Robo1/2* mutants. Thus the Eph/ephrin and Slit/Robo pathways seem to converge in neural progenitors to modulate early phases of neurogenesis. In particular, both pathways may contribute to maintain and expand the pool of VZ progenitors, favoring symmetrical cell divisions and preventing premature production of IPCs.

The mechanisms through which the Eph/ephrin and Slit/Robo pathways modulate cell proliferation may greatly vary, depending on the cellular context. For instance, EphB receptors regulate progenitor cell proliferation in the intestine via Abl and cyclin D1 (Genander et al., 2009) and Robo signaling has been shown to influence proliferation in the mammary epithelium through the regulation of the subcellular trafficking of b-catenin (Macias et al., 2011). Intriguingly, recent evidence suggests that ephrin signaling may influence cortical progenitor dynamics through a mechanism involving nuclear signaling, similar to what we have described here for Robo receptors. In cortical progenitors, the cytoplasmic domain of ephrin-B1 interacts with zinc-finger and homeodomain protein 2 (ZHX2), a transcriptional repressor, the activity of which is enhanced by ephrin-B1 signaling (Wu et al., 2009). These results suggest that transcriptional control might be a common mechanism of action of Eph/ephrin and Slit/Robo signaling on cortical progenitor cells.

Robo Signaling beyond Guidance

Although best known for its role in axon and dendrite guidance and branching, Robo signaling also has been implicated in leukocyte chemotaxis, tumor cell migration, and angiogenesis (Bauer et al., 2011; Legg et al., 2008; London and Li, 2011), as well as in other biological processes where its primary effect does not appear to be to regulate motility and the cytoskeleton, including kidney and cardiac development, mammary gland development, and myogenesis (Fish et al., 2011; Grieshammer et al., 2004; Kramer et al., 2001). Our study

indicates that Slits and their Robo receptors also modulate neural cell division in the developing brain, another biological process that does not seem to rely on the same molecular mechanisms that have been described for neuronal migration and axon guidance.

The identification of Robo genes as modulators of Notch signaling and neuronal progenitor proliferation uncovers a new signaling pathway that could potentially influence other cell types, such as stem cells or tumors. In this context, Slits and their respective receptors have been previously implicated in tumori-genesis via the regulation of cell migration, cell survival, and angiogenesis (Mehlen et al., 2011). In view of our findings, the possibility that Slit/Robo signaling may also contribute to tumor-igenesis through the abnormal regulation of cell proliferation should be experimentally tested.

EXPERIMENTAL PROCEDURES

Mouse Strains

Mice carrying loss-of-function alleles for *Robo1* and both *Robo1* and *Robo2* were maintained in an Institute for Cancer Research background, while *Robo2* mice were maintained in a C57b6 background. Mice were kept at the Instituto de Neurociencias de Alicante in accordance with Spanish and European Union regulations.

Immunohistochemistry and In Situ Hybridization

Twenty micrometer frozen brain sections were hybridized with digoxigenin-labeled probes, as described before (Flames et al., 2007). For immunohisto-chemistry of frozen or vibratome brain sections, the tissue was incubated with primary antibodies overnight, followed by appropriate secondary antibodies.

Slit Binding Experiments

The brains of wild-type embryos aged E12.5 were dissected out and incubated with concentrated conditioned medium containing Slit2-AP or control secretable AP, as described before (Fouquet et al., 2007).

Single Progenitor Clonal Analysis and Rescue Experiments

Retroviral stocks were prepared and concentrated as described previously (Zhao et al., 2006). Embryos were injected with 200 nl of *Gfp*-encoding retroviruses (5×10^6 cfu/ml) into the telencephalic ventricles using an ultra-sound backscatter microscope, as previously described (Pla et al., 2006). For testing cell-autonomy, E11.5 wild-type embryos were injected with retroviruses encoding a dominant negative form of *Robo2* along with *Gfp* (*DN-Robo2-IRES-Gfp*). For gain of function experiments, E12.5 wild-type embryos were electroporated in utero with a plasmid encoding a myristoylated form of the cytoplasmic domain of *Robo2* (*mR2*). For *Hes1* rescue experiments, E12.5 embryos were electroporated in utero with plasmids encoding *Hes1* and *Gfp* or *Gfp* alone. For *Hes1* RNA interference (RNAi) experiments, E12.5 wild-type embryos were electroporated in utero with a cocktail of two siRNA that have been previously shown to produce significant knockdown of mouse *Hes1* (Noda et al., 2011; Ross et al., 2004) or with control siRNA.

Primary Dissociated Cell Cultures

E12.5 neocortical tissue was incubated in trypsin-EDTA and DNase at 37° C for 6 min, followed by gentle trituration. Dissociated cells were plated on glass coverslips coated with poly-lysine and laminin at a density of 4,500 cells/mm^2 and were cultured in Neurobasal medium and incubated at 37° C in 95% humidity, 5% CO_2.

Luciferase Assays

Primary dissociated cell cultures were transfected after 48 hr in culture using Lipofectamine 2000 (Invitrogen). Two days after transfection, cells were collected and treated for the detection of luciferase and renilla activity using the Dual-Luciferase Reporter Assay (Promega).

Semiquantitative RT-PCR and qPCR

Total RNA from E12.5 cortex and basal ganglia was extracted using the RNeasy Mini Kit (QIAGEN). A total of 500 ng RNA was treated with DNaseI RNase-free (Fermentas) for 30 min at 37° C prior to reverse transcription into single-stranded complementary DNA using SuperScriptII Reverse Transcriptase and Oligo(dT)$_{12\text{-}18}$ primers (Invitrogen) for 1 hr at 42° C. For quantitative (q) PCR, total RNA was extracted from E12.5 cortical slices and qPCR was carried out in an Applied Biosystems 7300 real-time PCR unit using the Platinum SYBR Green qPCR Supermix UDG with ROX (Invitrogen) or TaqMan probes (Life Technologies).

Western Blot and Dot Blot

For detection of Robo1 and Robo2 in E10.5 mouse, the telencephalon of eight embryos was collected. Membranes were probed with anti-Robo1 (a kind gift of F. Murakami) and anti-Robo2 (R&D Systems) antibodies. For the detection of Slit ligands in the CSF, 10 μl CSF from the lateral ventricles of E12.5 embryos or from COS cell-conditioned medium were adsorbed onto nitrocellulose membranes in a single dot and probed with a recombinant human ROBO2-Fc chimera (R&D Systems).

Quantification and Statistics *Volume, Thickness, and Length Measurements*

Cavalieri estimates of the volume of the whole telencephalon and thalamus were measured using StereoInvestigator software (Microbrightfield). Total thickness of the cerebral cortex, or thickness of the TUJ1+ or BrdU+ layer, and length of the VZ were measured from DAPI-stained or immunostained coronal sections using ImageJ software.

Cell Counts—Cells were counted from the entire mediolateral extent of the dorso-parietal neocortex and at mid-rostrocaudal levels, identical between controls and mutants. For each section, the total cell count was normalized to the length of the VZ. For cleaved Caspase-3, all positive nuclei were counted, regardless of their apicobasal position. For Tbr2, all positive nuclei located outside of the TUJ1+ layer were counted. For studies of colocalization, single plane images were obtained using a Leica TCS SL confocal microscope and analyzed with Leica Confocal Software.

N-Cadherin and Apical Surface Measurements—Levels of N-Cadherin immunoreactivity (measured as mean gray value) and thickness of apical band for adherens junction proteins were measured on single plane confocal images using ImageJ.

Calculation of Ratio-to-Control and Criterion for Phenotypic Penetrance—Phenotypic penetrance was variable in different litters of mutant embryos, but roughly 60%–70% of the mutant embryos analyzed displayed the phenotypes described in this study. For each litter independently, the mean value among control embryos was calculated. This was then used to calculate the ratio-to-control, defined as the ratio between the measurement on each embryo and the mean value among controls for that litter. Next we measured the SD of this ratio-to-control among control embryos from all litters pooled. The ratio-to-control was then calculated for all mutant embryos, each referred to the mean control value of its own litter. Those mutant embryos with a ratio-to-control value closer than 1 SD to the control average were considered phenotypically nonpenetrant. For the remaining, the mean and SEM of ratio-to-control was calculated.

Data were statistically analyzed with SPSS software using χ^2-test, pair-wise t test, or independent samples t test, where appropriate. Histograms represent mean ± SEM.

Supplementary Material

Refer to Web version on PubMed Central for supplementary material.

ACKNOWLEDGMENTS

REFERENCES

Andrews W, Barber M, Hernadez-Miranda LR, Xian J, Raki S, Sundaresan V, Rabbitts TH, Pannell R, Rabbitts P, Thompson H, et al. The role of Slit-Robo signaling in the generation, migration and morphological differentiation of cortical interneurons. Dev. Biol. 2008; 313:648–658. [PubMed: 18054781]

Arai Y, Pulvers JN, Haffner C, Schilling B, Nüsslein I, Calegari F, Huttner WB. Neural stem and progenitor cells shorten S-phase on commitment to neuron production. Nat. Commun. 2011; 2:154. [PubMed: 21224845]

Bagri A, Marín O, Plump AS, Mak J, Pleasure SJ, Rubenstein JL, Tessier-Lavigne M. Slit proteins prevent midline crossing and determine the dorsoventral position of major axonal pathways in the mammalian forebrain. Neuron. 2002; 33:233–248. [PubMed: 11804571]

Bai G, Chivatakarn O, Bonanomi D, Lettieri K, Franco L, Xia C, Stein E, Ma L, Lewcock JW, Pfaff SL. Presenilin-dependent receptor processing is required for axon guidance. Cell. 2011; 144:106–118. [PubMed: 21215373]

Bashaw GJ, Kidd T, Murray D, Pawson T, Goodman CS. Repulsive axon guidance: Abelson and Enabled play opposing roles down-stream of the roundabout receptor. Cell. 2000; 101:703–715. [PubMed: 10892742]

Bauer K, Dowejko A, Bosserhoff AK, Reichert TE, Bauer R. Slit-2 facilitates interaction of P-cadherin with Robo-3 and inhibits cell migration in an oral squamous cell carcinoma cell line. Carcinogenesis. 2011; 32:935–943. [PubMed: 21459757]

Brose K, Tessier-Lavigne M. Slit proteins: key regulators of axon guidance, axonal branching, and cell migration. Curr. Opin. Neurobiol. 2000; 10:95–102. [PubMed: 10679444]

Brose K, Bland KS, Wang KH, Arnott D, Henzel W, Goodman CS, Tessier-Lavigne M, Kidd T. Slit proteins bind Robo receptors and have an evolutionarily conserved role in repulsive axon guidance. Cell. 1999; 96:795–806. [PubMed: 10102268]

Cappello S, Attardo A, Wu X, Iwasato T, Itohara S, Wilsch-Bräuninger M, Eilken HM, Rieger MA, Schroeder TT, Huttner WB, et al. The Rho-GTPase cdc42 regulates neural progenitor fate at the apical surface. Nat. Neurosci. 2006; 9:1099–1107. [PubMed: 16892058]

Chumley MJ, Catchpole T, Silvany RE, Kernie SG, Henkemeyer M. EphB receptors regulate stem/ progenitor cell proliferation, migration, and polarity during hippocampal neurogenesis. J. Neurosci. 2007; 27:13481–13490. [PubMed: 18057206]

Conover JC, Doetsch F, Garcia-Verdugo JM, Gale NW, Yancopoulos GD, Alvarez-Buylla A. Disruption of Eph/ephrin signaling affects migration and proliferation in the adult subventricular zone. Nat. Neurosci. 2000; 3:1091–1097. [PubMed: 11036265]

Depaepe V, Suarez-Gonzalez N, Dufour A, Passante L, Gorski JA, Jones KR, Ledent C, Vanderhaeghen P. Ephrin signalling controls brain size by regulating apoptosis of neural progenitors. Nature. 2005; 435:1244–1250. [PubMed: 15902206]

Dickson BJ, Gilestro GF. Regulation of commissural axon path-finding by slit and its Robo receptors. Annu. Rev. Cell Dev. Biol. 2006; 22:651–675. [PubMed: 17029581]

Farkas LM, Haffner C, Giger T, Khaitovich P, Nowick K, Birchmeier C, Pääbo S, Huttner WB. Insulinoma-associated 1 has a panneurogenic role and promotes the generation and expansion of basal progenitors in the developing mouse neocortex. Neuron. 2008; 60:40–55. [PubMed: 18940587]

Fietz SA, Huttner WB. Cortical progenitor expansion, self-renewal and neurogenesis-a polarized perspective. Curr. Opin. Neurobiol. 2011; 21:23–35. [PubMed: 21036598]

Fish JE, Wythe JD, Xiao T, Bruneau BG, Stainier DY, Srivastava D, Woo S. A Slit/miR-218/Robo regulatory loop is required during heart tube formation in zebrafish. Development. 2011; 138:1409–1419. [PubMed: 21385766]

Flames N, Pla R, Gelman DM, Rubenstein JL, Puelles L, Marín O. Delineation of multiple subpallial progenitor domains by the combinatorial expression of transcriptional codes. J. Neurosci. 2007; 27:9682–9695. [PubMed: 17804629]

Fouquet C, Di Meglio T, Ma L, Kawasaki T, Long H, Hirata T, Tessier-Lavigne M, Chédotal A, Nguyen-Ba-Charvet KT. Robo1 and robo2 control the development of the lateral olfactory tract. J. Neurosci. 2007; 27:3037–3045. [PubMed: 17360927]

Franklin JL, Berechid BE, Cutting FB, Presente A, Chambers CB, Foltz DR, Ferreira A, Nye JS. Autonomous and non-autonomous regulation of mammalian neurite development by Notch1 and Delta1. Curr. Biol. 1999; 9:1448–1457. [PubMed: 10607588]

Genander M, Frisén J. Ephrins and Eph receptors in stem cells and cancer. Curr. Opin. Cell Biol. 2010; 22:611–616. [PubMed: 20810264]

Genander M, Halford MM, Xu NJ, Eriksson M, Yu Z, Qiu Z, Martling A, Greicius G, Thakar S, Catchpole T, et al. Dissociation of EphB2 signaling pathways mediating progenitor cell proliferation and tumor suppression. Cell. 2009; 139:679–692. [PubMed: 19914164]

Grieshammer U, Ma, Le, Plump AS, Wang F, Tessier-Lavigne M, Martin GR. SLIT2-mediated ROBO2 signaling restricts kidney induction to a single site. Dev. Cell. 2004; 6:709–717. [PubMed: 15130495]

Hämmerle B, Tejedor FJ. A novel function of DELTA-NOTCH signalling mediates the transition from proliferation to neurogenesis in neural progenitor cells. PLoS ONE. 2007; 2:e1169. [PubMed: 18000541]

Hansen DV, Lui JH, Parker PR, Kriegstein AR. Neurogenic radial glia in the outer subventricular zone of human neocortex. Nature. 2010; 464:554–561. [PubMed: 20154730]

Haubensak W, Attardo A, Denk W, Huttner WB. Neurons arise in the basal neuroepithelium of the early mammalian telencephalon: a major site of neurogenesis. Proc. Natl. Acad. Sci. USA. 2004; 101:3196–3201. [PubMed: 14963232]

Holmberg J, Armulik A, Senti KA, Edoff K, Spalding K, Momma S, Cassidy R, Flanagan JG, Frisén J. Ephrin-A2 reverse signaling negatively regulates neural progenitor proliferation and neurogenesis. Genes Dev. 2005; 19:462–471. [PubMed: 15713841]

Hu H. Cell-surface heparan sulfate is involved in the repulsive guidance activities of Slit2 protein. Nat. Neurosci. 2001; 4:695–701. [PubMed: 11426225]

Hu H, Li M, Labrador JP, McEwen J, Lai EC, Goodman CS, Bashaw GJ. Cross GTPase-activating protein (CrossGAP)/Vilse links the Roundabout receptor to Rac to regulate midline repulsion. Proc. Natl. Acad. Sci. USA. 2005; 102:4613–4618. [PubMed: 15755809]

Huttner WB, Kosodo Y. Symmetric versus asymmetric cell division during neurogenesis in the developing vertebrate central nervous system. Curr. Opin. Cell Biol. 2005; 17:648–657. [PubMed: 16243506]

Ishibashi M, Moriyoshi K, Sasai Y, Shiota K, Nakanishi S, Kageyama R. Persistent expression of helix-loop-helix factor HES-1 prevents mammalian neural differentiation in the central nervous system. EMBO J. 1994; 13:1799–1805. [PubMed: 7909512]

Kang W, Wong LC, Shi SH, Hébert JM. The transition from radial glial to intermediate progenitor cell is inhibited by FGF signaling during corticogenesis. J. Neurosci. 2009; 29:14571–14580. [PubMed: 19923290]

Kawaguchi A, Ikawa T, Kasukawa T, Ueda HR, Kurimoto K, Saitou M, Matsuzaki F. Single-cell gene profiling defines differential progenitor subclasses in mammalian neurogenesis. Development. 2008; 135:3113–3124. [PubMed: 18725516]

Kidd T, Brose K, Mitchell KJ, Fetter RD, Tessier-Lavigne M, Goodman CS, Tear G. Roundabout controls axon crossing of the CNS midline and defines a novel subfamily of evolutionarily conserved guidance receptors. Cell. 1998; 92:205–215. [PubMed: 9458045]

Kidd T, Bland KS, Goodman CS. Slit is the midline repellent for the robo receptor in Drosophila. Cell. 1999; 96:785–794. [PubMed: 10102267]

Kramer SG, Kidd T, Simpson JH, Goodman CS. Switching repulsion to attraction: changing responses to slit during transition in mesoderm migration. Science. 2001; 292:737–740. [PubMed: 11326102]

Legg JA, Herbert JM, Clissold P, Bicknell R. Slits and Roundabouts in cancer, tumour angiogenesis and endothelial cell migration. Angiogenesis. 2008; 11:13–21. [PubMed: 18264786]

Lehtinen MK, Zappaterra MW, Chen X, Yang YJ, Hill AD, Lun M, Maynard T, Gonzalez D, Kim S, Ye P, et al. The cerebrospinal fluid provides a proliferative niche for neural progenitor cells. Neuron. 2011; 69:893–905. [PubMed: 21382550]

Li HS, Chen JH, Wu W, Fagaly T, Zhou L, Yuan W, Dupuis S, Jiang ZH, Nash W, Gick C, et al. Vertebrate slit, a secreted ligand for the transmembrane protein roundabout, is a repellent for olfactory bulb axons. Cell. 1999; 96:807–818. [PubMed: 10102269]

London NR, Li DY. Robo4-dependent Slit signaling stabilizes the vasculature during pathologic angiogenesis and cytokine storm. Curr. Opin. Hematol. 2011; 18:186–190. [PubMed: 21423011]

Long H, Sabatier C, Ma L, Plump A, Yuan W, Ornitz DM, Tamada A, Murakami F, Goodman CS, Tessier-Lavigne M. Conserved roles for Slit and Robo proteins in midline commissural axon guidance. Neuron. 2004; 42:213–223. [PubMed: 15091338]

López-Bendito G, Flames N, Ma L, Fouquet C, Di Meglio T, Chedotal A, Tessier-Lavigne M, Marín O. Robo1 and Robo2 cooperate to control the guidance of major axonal tracts in the mammalian forebrain. J. Neurosci. 2007; 27:3395–3407. [PubMed: 17392456]

Macias H, Moran A, Samara Y, Moreno M, Compton JE, Harburg G, Strickland P, Hinck L. SLIT/ROBO1 signaling suppresses mammary branching morphogenesis by limiting basal cell number. Dev. Cell. 2011; 20:827–840. [PubMed: 21664580]

Marillat V, Cases O, Nguyen Ba-Charvet KT, Tessier-Lavigne M, Sotelo C, Chédotal A. Spatiotemporal expression patterns of slit and robo genes in the rat brain. J. Comp. Neurol. 2001; 442:130–155. [PubMed: 11754167]

Mehlen P, Delloye-Bourgeois C, Chédotal A. Novel roles for Slits and netrins: axon guidance cues as anticancer targets? Nat. Rev. Cancer. 2011; 11:188–197. [PubMed: 21326323]

Mehta B, Bhat KM. Slit signaling promotes the terminal asymmetric division of neural precursor cells in the Drosophila CNS. Development. 2001; 128:3161–3168. [PubMed: 11688564]

Mizutani KI, Yoon K, Dang L, Tokunaga A, Gaiano N. Differential Notch signalling distinguishes neural stem cells from intermediate progenitors. Nature. 2007; 449:351–355. [PubMed: 17721509]

Nakamura Y, Sakakibara S, Miyata T, Ogawa M, Shimazaki T, Weiss S, Kageyama R, Okano H. The bHLH gene hes1 as a repressor of the neuronal commitment of CNS stem cells. J. Neurosci. 2000; 20:283–293. [PubMed: 10627606]

Noctor SC, Flint AC, Weissman TA, Wong WS, Clinton BK, Kriegstein AR. Dividing precursor cells of the embryonic cortical ventricular zone have morphological and molecular characteristics of radial glia. J. Neurosci. 2002; 22:3161–3173. [PubMed: 11943818]

Noctor SC, Martínez-Cerdeño V, Ivic L, Kriegstein AR. Cortical neurons arise in symmetric and asymmetric division zones and migrate through specific phases. Nat. Neurosci. 2004; 7:136–144. [PubMed: 14703572]

Noctor SC, Martínez-Cerdeño V, Kriegstein AR. Contribution of intermediate progenitor cells to cortical histogenesis. Arch. Neurol. 2007; 64:639–642. [PubMed: 17502462]

Noctor SC, Martínez-Cerdeño V, Kriegstein AR. Distinct behaviors of neural stem and progenitor cells underlie cortical neurogenesis. J. Comp. Neurol. 2008; 508:28–44. [PubMed: 18288691]

Noda N, Honma S, Ohmiya Y. Hes1 is required for contact inhibition of cell proliferation in 3T3-L1 preadipocytes. Genes Cells. 2011; 16:704–713. [PubMed: 21481105]

Pla R, Borrell V, Flames N, Marín O. Layer acquisition by cortical GABAergic interneurons is independent of Reelin signaling. J. Neurosci. 2006; 26:6924–6934. [PubMed: 16807322]

Plump AS, Erskine L, Sabatier C, Brose K, Epstein CJ, Goodman CS, Mason CA, Tessier-Lavigne M. Slit1 and Slit2 cooperate to prevent premature midline crossing of retinal axons in the mouse visual system. Neuron. 2002; 33:219–232. [PubMed: 11804570]

Pontious A, Kowalczyk T, Englund C, Hevner RF. Role of intermediate progenitor cells in cerebral cortex development. Dev. Neurosci. 2008; 30:24–32. [PubMed: 18075251]

Qiu R, Wang X, Davy A, Wu C, Murai K, Zhang H, Flanagan JG, Soriano P, Lu Q. Regulation of neural progenitor cell state by ephrin-B. J. Cell Biol. 2008; 181:973–983. [PubMed: 18541704]

Redmond L, Oh SR, Hicks C, Weinmaster G, Ghosh A. Nuclear Notch1 signaling and the regulation of dendritic development. Nat. Neurosci. 2000; 3:30–40. [PubMed: 10607392]

Rhee J, Mahfooz NS, Arregui C, Lilien J, Balsamo J, VanBerkum MF. Activation of the repulsive receptor Roundabout inhibits N-cadherin-mediated cell adhesion. Nat. Cell Biol. 2002; 4:798–805. [PubMed: 12360290]

Rhee J, Buchan T, Zukerberg L, Lilien J, Balsamo J. Cables links Robo-bound Abl kinase to N-cadherin-bound beta-catenin to mediate Slit-induced modulation of adhesion and transcription. Nat. Cell Biol. 2007; 9:883–892. [PubMed: 17618275]

Ross DA, Rao PK, Kadesch T. Dual roles for the Notch target gene Hes-1 in the differentiation of 3T3-L1 preadipocytes. Mol. Cell. Biol. 2004; 24:3505–3513. [PubMed: 15060169]

Skeath JB, Thor S. Genetic control of Drosophila nerve cord development. Curr. Opin. Neurobiol. 2003; 13:8–15. [PubMed: 12593977]

Stein E, Tessier-Lavigne M. Hierarchical organization of guidance receptors: silencing of netrin attraction by slit through a Robo/DCC receptor complex. Science. 2001; 291:1928–1938. [PubMed: 11239147]

Wang KH, Brose K, Arnott D, Kidd T, Goodman CS, Henzel W, Tessier-Lavigne M. Biochemical purification of a mammalian slit protein as a positive regulator of sensory axon elongation and branching. Cell. 1999; 96:771–784. [PubMed: 10102266]

Whitford KL, Marillat V, Stein E, Goodman CS, Tessier-Lavigne M, Chédotal A, Ghosh A. Regulation of cortical dendrite development by Slit-Robo interactions. Neuron. 2002; 33:47–61. [PubMed: 11779479]

Wong K, Ren XR, Huang YZ, Xie Y, Liu G, Saito H, Tang H, Wen L, Brady-Kalnay SM, Mei L, et al. Signal transduction in neuronal migration: roles of GTPase activating proteins and the small GTPase Cdc42 in the Slit-Robo pathway. Cell. 2001; 107:209–221. [PubMed: 11672528]

Wong GK, Baudet ML, Norden C, Leung L, Harris WA. Slit1b-Robo3 signaling and N-cadherin regulate apical process retraction in developing retinal ganglion cells. J. Neurosci. 2012; 32:223–228. [PubMed: 22219284]

Wu C, Qiu R, Wang J, Zhang H, Murai K, Lu Q. ZHX2 Interacts with Ephrin-B and regulates neural progenitor maintenance in the developing cerebral cortex. J. Neurosci. 2009; 29:7404–7412. [PubMed: 19515908]

Yang L, Bashaw GJ. Son of sevenless directly links the Robo receptor to rac activation to control axon repulsion at the midline. Neuron. 2006; 52:595–607. [PubMed: 17114045]

Ypsilanti AR, Zagar Y, Chédotal A. Moving away from the midline: new developments for Slit and Robo. Development. 2010; 137:1939–1952. [PubMed: 20501589]

Zhao C, Teng EM, Summers RG Jr. Ming GL, Gage FH. Distinct morphological stages of dentate granule neuron maturation in the adult mouse hippocampus. J. Neurosci. 2006; 26:3–11. [PubMed: 16399667]

Zhou WJ, Geng ZH, Chi S, Zhang W, Niu XF, Lan SJ, Ma L, Yang X, Wang LJ, Ding YQ, Geng JG. Slit-Robo signaling induces malignant transformation through Hakai-mediated E-cadherin degradation during colorectal epithelial cell carcinogenesis. Cell Res. 2011; 21:609–626. [PubMed: 21283129]
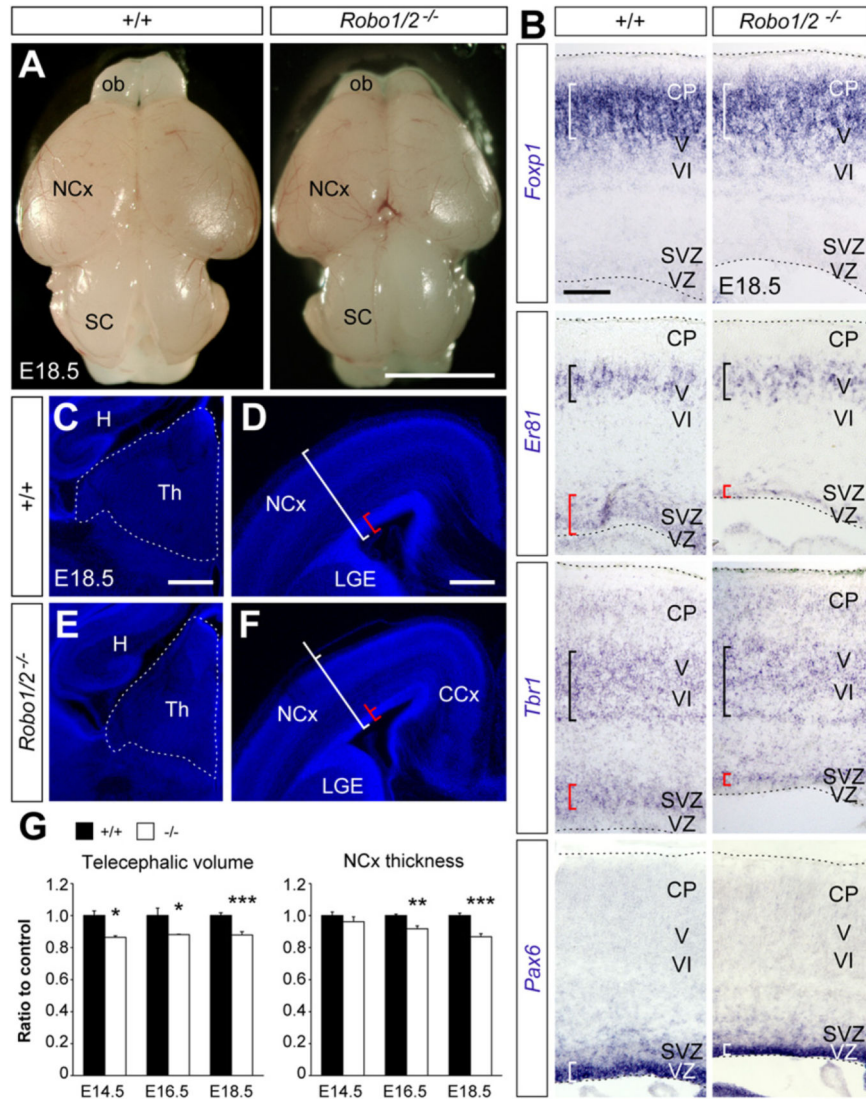
Figure 1. Reduced Size of Brain Structures in *Robo1/2* Mutants at E18.5

(A) External view of brains from control and mutant embryos. Note the reduced size of the neocortex (NCx) and olfactory bulb.

(B) Patterns of mRNA expression for *Foxp1*, *Er81*, *Tbr1*, and *Pax6* in the cerebral cortex of control and mutant embryos. White and black brackets indicate the thickness and position of the neuronal layers with the darkest stain; red brackets indicate thickness of the proliferative layer as revealed by the dim stain.

(C–F) Coronal sections of the thalamus (C and E) and NCx (D and F) in control and mutants stained with DAPI. White and red brackets serve as reference of the thickness of the neocortex and proliferative layer seen in controls.

(G) Quantification of brain morphometric parameters between E14.5 and E18.5 in control (+/+) and mutants (-/-). Values are expressed as relative to measurements in control embryos; mean ± SEM (n = 4–11 embryos per group), t test, *p < 0.05; **p < 0.01; ***p < 0.001.

Scale bars equal 3 cm (A), 200 μm (B), and 350 μm (C–F). CCx, cingulated cortex; H, hippocampus; ob, olfactory bulb; SC, superior colliculus; Th, thalamus. See also Figure S1.
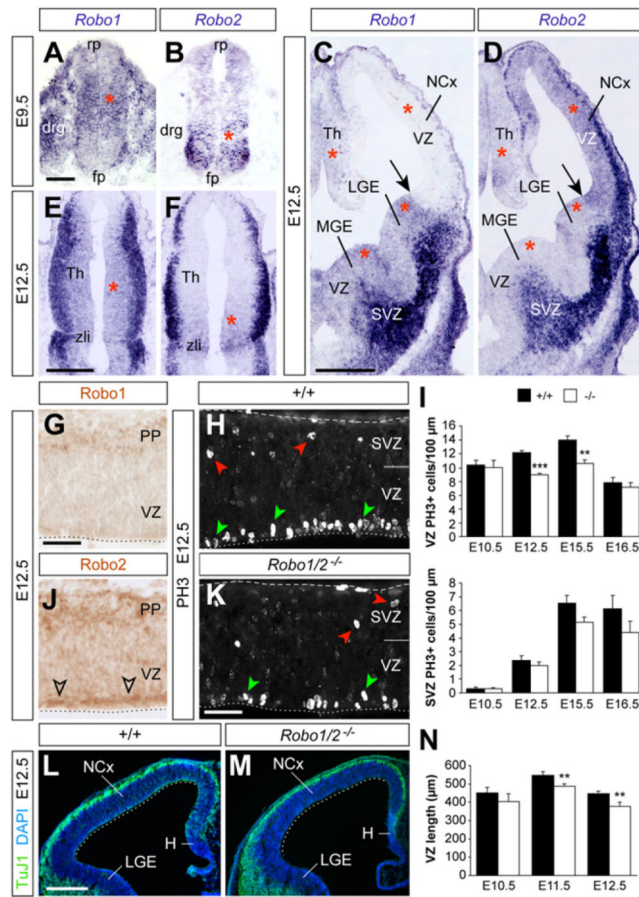
**Figure 2. Robo1 and Robo2 Are Expressed in CNS Progenitors and Are Required to Sustain Ventricular Mitosis**

(A–F) Coronal sections through the spinal cord (A and B), telencephalon (C and D), and thalamus (E and F), showing expression of *Robo1* and *Robo2* mRNA at the indicated ages. Arrows point at the pallial-subpallial boundary. Red asterisks mark progenitor regions.

(G and J) Immunohistochemistry for Robo1 and Robo2 in the E12.5 NCx. (H and K) PH3 stains in the E12.5 neocortex of control and mutant embryos. Green arrowheads indicate VZ mitoses; red arrowheads indicate SVZ mitoses. (I) Quantification of linear density of PH3+ nuclei in the VZ and SVZ of controls (+/+) and *Robo1/2* mutants (-/-) at different stages; mean ± SEM (n = 4–6 embryos per group).

(L and M) TuJ1/DAPI stains in the E12.5 NCx of control and mutant embryos.

(N) Quantification of the length of the pallial VZ, as indicated by the dotted lines in (L) and (M). Mean ± SEM (n = 4–7 embryos per group). t test; **$p < 0.01$; ***$p < 0.001$.

Scale bars equal 50 μm (A and B), 500 μm (C–F, L and M), and 100 μm (G–K). drg, dorsal root ganglion; fp, floor plate; PP, preplate; rp, roof plate; zli, zonal limitans intrathalamica. See also Figures S2 and S3.
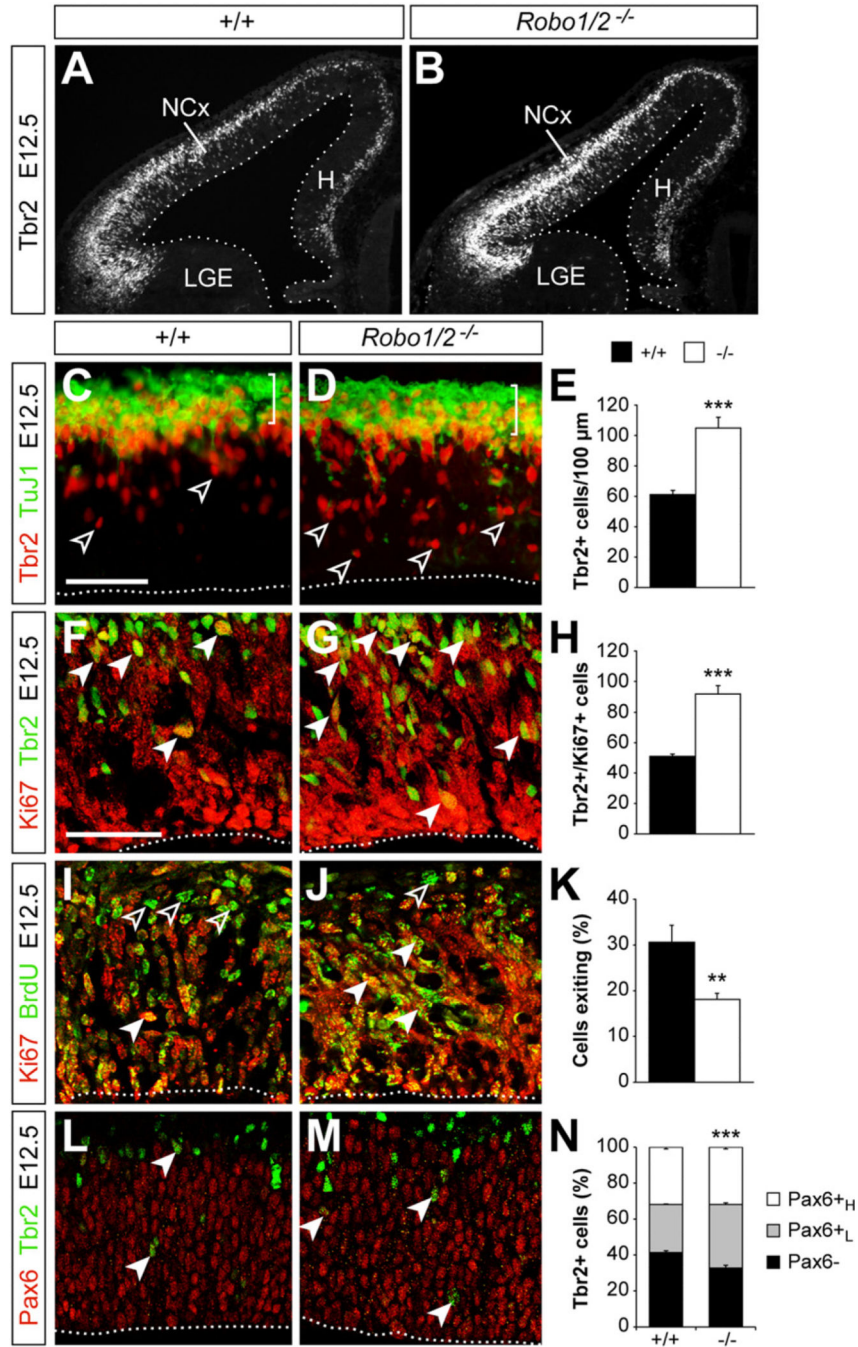
Figure 3. Robo Receptors Modulate the Dynamics of Cortical Intermediate Progenitors
Tbr2 expression in the cortex of control and mutant embryos at E12.5 (A and B).
Distribution of TuJ1+ neurons and Tbr2+ cells (C and D), cycling Tbr2+/Ki67+ cells (F and G), cell exiting cycle exit (I and J), and Tbr2/Pax6 coexpression (L and M) in the NCx of control and mutant embryos at E12.5. Open arrowheads indicate Tbr2+ cells (C and D) or Ki67–/BrdU+ cells (I and J). Solid arrowheads point to Ki67+/Tbr2 double-labeled cells (F and G), Ki67+/BrdU+ double-labeled cells (I and J), and Pax6+/Tbr2+ double-labeled cells (L and M). For Ki67/BrdU experiments, BrdU was injected 24 hr prior to sacrifice.

Quantification of the density of Tbr2+ cells (E), the density of Tbr2+/Ki67+ cells (H), the fraction of cells exiting the cell cycle (K), and the fraction of Tbr2+ cells expressing Pax6 at high ($Pax6_H$) or low levels ($Pax6_L$) (N) in control and *Robo1/2* mutants. Mean ± SEM (n = 4–5 animals per group). For cell-cycle exit (K) and % Tbr2+ cells (N), χ^2-test; for all other comparisons, t test; **p < 0.01; ***p < 0.001. Scale bars equal 50 μm. See also Figures S4 and S6.
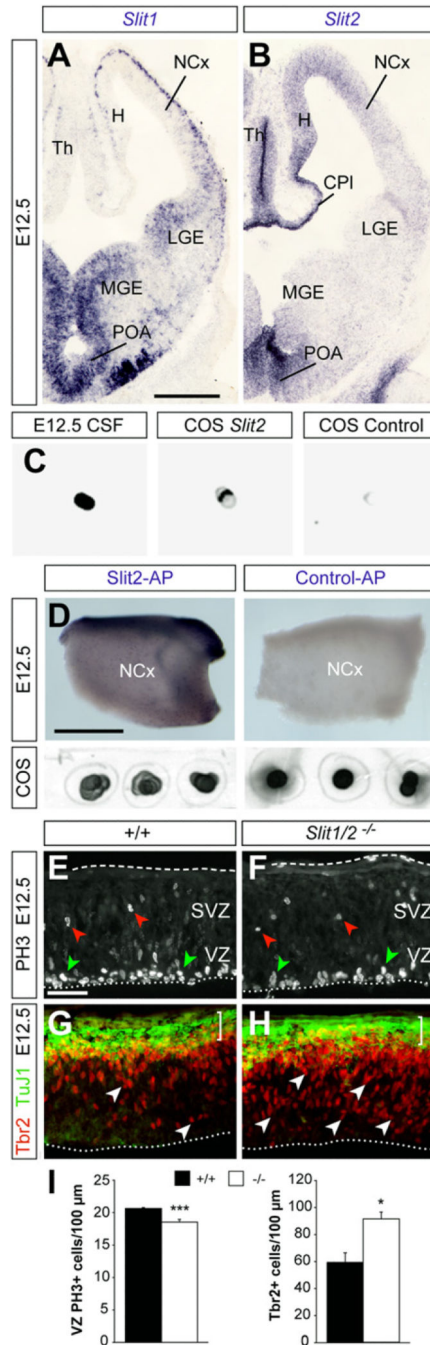
Figure 4. Altered Neurogenesis in the Cortex of *Slit1/2* Mutants

(A and B) Coronal sections through the telencephalon, showing expression of *Slit1* and *Slit2* mRNA at E12.5.

(C) Dot blot analysis of Robo ligands in the CSF of E12.5 mouse embryos.

(D) Open-book preparation of whole telencephalic hemispheres stained for alkaline phosphatase enzyme with Slit2-AP or control AP probes. Dot blots reveal that the level of AP expression in COS cells transfected with Slit2-AP or control-AP is similar.

(E and F) PH3 stains in the NCx in control and *Slit1/2* mutant embryos at E12.5. Green and red arrowheads indicate PH3+ nuclei in the VZ and SVZ, respectively.

(G and H) Tbr2 stains in the NCx of control and *Slit1/2* mutant embryos at E12.5. Open arrowheads point to IPCs.

(I) Quantification of the density of PH3+ nuclei in the VZ and Tbr2+ nuclei in control and *Slit1/2* mutants. Mean ± SEM (n = 3–5 embryos per group). t test, *p < 0.05; ***p < 0.001. CPl, choroid plexus; H, hippocampus; POA, preoptic area. Scale bars equal 250 μm. See also Figure S5.
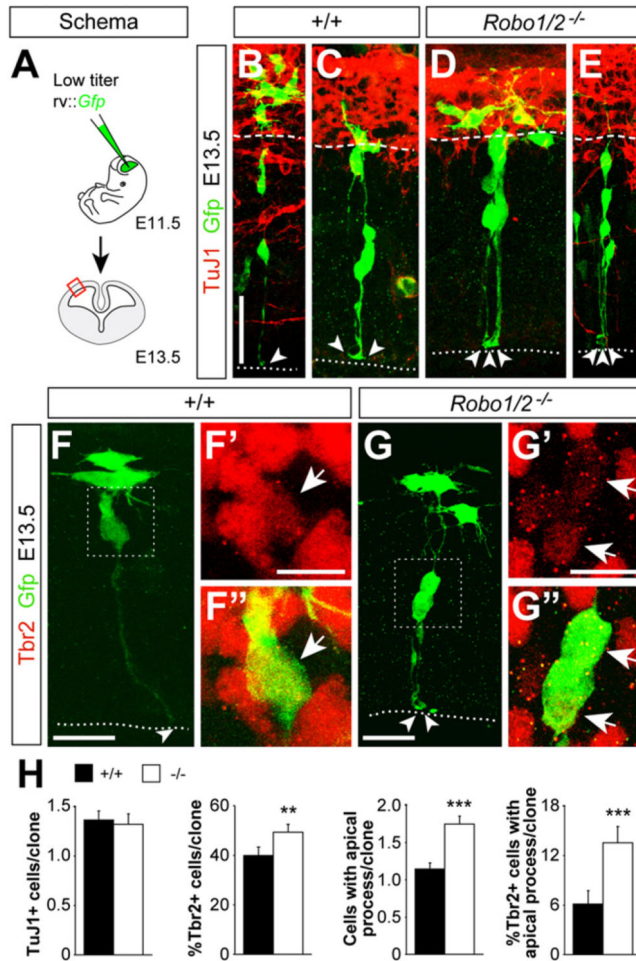
Figure 5. Clonal Analysis of Progenitor Dynamics in *Robo1/2* Mutants

(A) Experimental paradigm used for cortical progenitor clonal analysis.

(B–G″) Analysis of individual clones in the E13.5 neocortex of control and mutant embryos labeled after retrovirus injection at E11.5. Within clones, cells were classified for TuJ1 (B–E) and Tbr2 (F–G″) immunoreactivity. The intensity of Tbr2 staining was very variable, but even cells with low Tbr2 levels were clearly distinguishable from nearby negative cells. Boxes in (F) and (G) indicate areas shown in (F′) and (F″) and (G′) and (G″), respectively. Dotted lines delineate the ventricular border, dashed lines delineate the border between TuJ1+ and TuJ1 cells, and arrowheads indicate the end feet of apical processes.

(H) Quantification of the number of TuJ1+ cells, percent of Tbr2+ cells, number of cells with an apical process, and percent of Tbr2+ cells with an apical process, per cortical clone. Mean ± SEM (n = 206 control clones from five different embryos; n = 186 mutant clones from four different embryos). For Tbr2+ cells, and Tbr2+ cells with apical process in clones, χ^2-test; for all other comparisons, t test. $**p < 0.01$; $***p < 0.001$.

Scale bars equal 30 μm (B and E), 20 μm (C and D), 15 μm (F and G), and 7 μm (F′, F″, G′, and G″). See also Figure S7.
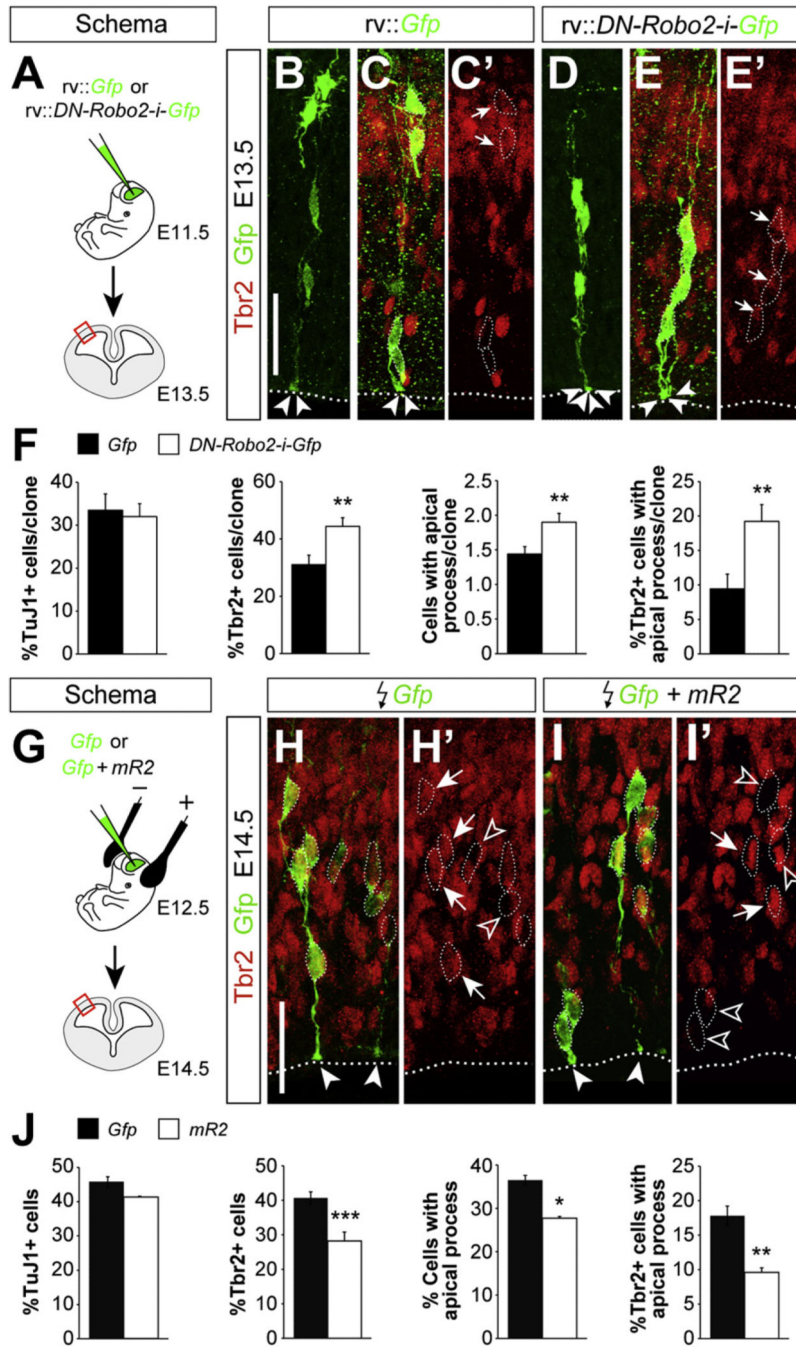
Figure 6. Robo Signaling Influences the Generation of IPCs in a Cell-Autonomous Manner

(A) Experimental paradigm used for the analysis of cell autonomy.

(B–E″) Analysis of individual clones in the E13.5 neocortex of wild-type embryos labeled after control (rv::*Gfp*) or dominant negative Robo2 (rv::*DN-Robo2-ires-Gfp*) retrovirus injection at E11.5. Within individual clones, cells were classified for TuJ1 and Tbr2 (B–E′) immunoreactivity, as well as for the presence of an apical process. Dotted lines delineate the ventricular border, arrows point to Tbr2+ cells, and arrowheads indicate the end feet of apical processes.

(F) Quantification of the number of TuJ1+ cells, percent of Tbr2+ cells, number of cells with an apical process, and percent of Tbr2+ cells with an apical process, per cortical clone. Mean ± SEM (Gfp: n = 107 clones from three different embryos; DN-Robo2: n = 148 clones from four different embryos).

(G) Experimental paradigm used for the analysis of gain of function.

(H–I′) Coronal sections through the cortex of E14.5 wild-type embryos showing Gfp and Tbr2 stains after electroporation with *Gfp* or *Gfp + mR2* at E12.5. Images are full stacks of confocal planes. Arrows and open arrowheads point to Tbr2+ and Tbr2– cells, respectively, as assessed from individual confocal plane images. Solid arrowheads indicate the end feet of apical processes.

(J) Quantification of the number of TuJ1+ cells, percent of Tbr2+ cells, number of cells with an apical process, and percent of Tbr2+ cells with an apical process among the electroporated (Gfp+) cells. Mean ± SEM (Gfp: n = 1533 cells from five different embryos; Gfp + mR2: n = 1462 cells from three different embryos).

For Tbr2+ cells and Tbr2+ cells with apical process in clones, χ^2-test; for all other comparisons, t test. *p < 0.05; **p < 0.01; ***p < 0.001. Scale bars equal 40 μm (B–E′) and 30 μm (H–I′).
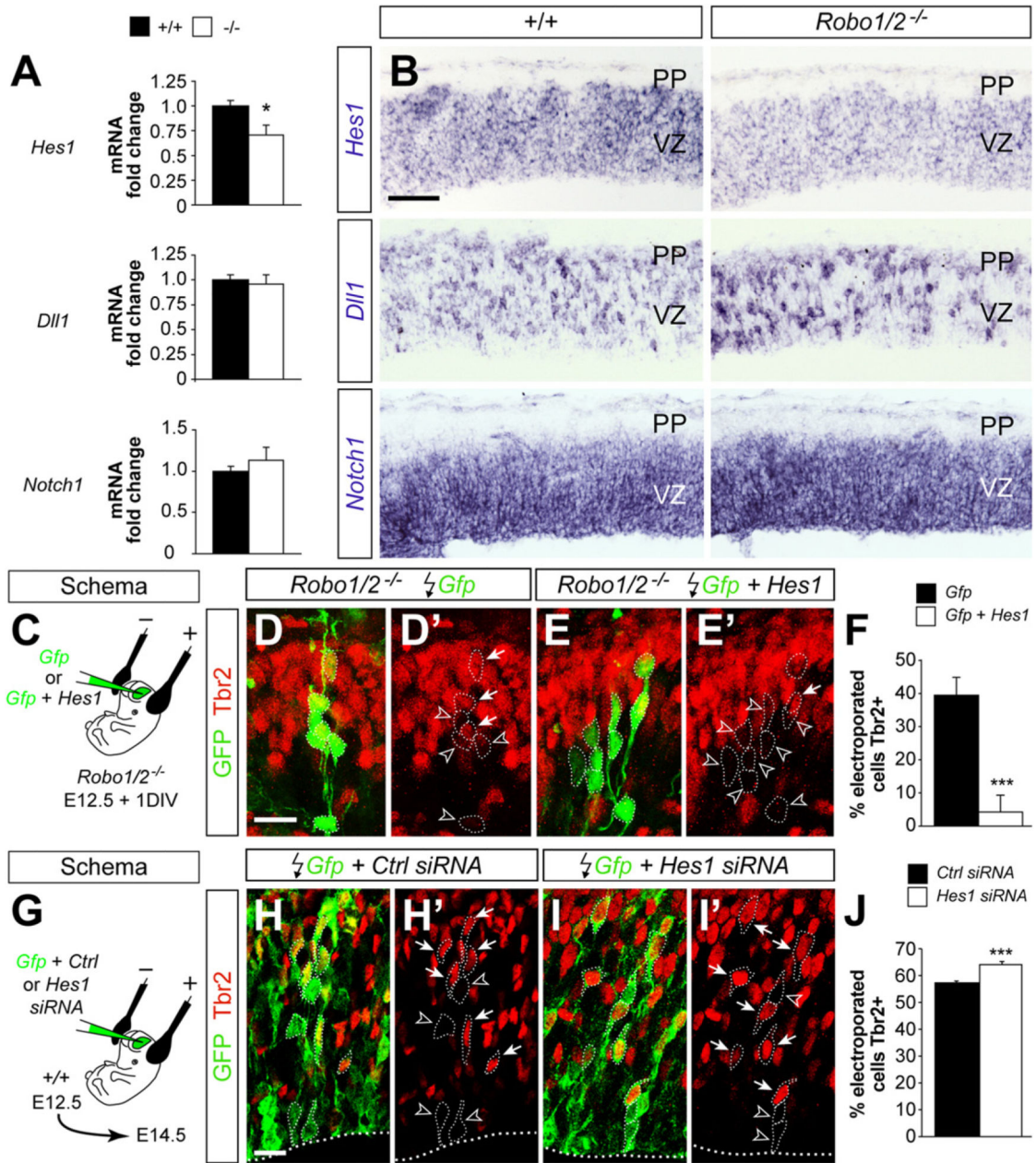
Figure 7. Robo Signaling Is Required for Normal *Hes1* mRNA Expression

(A) qPCR measurements of *Hes1*, *Dll1*, and *Notch1* mRNA expressed as values relative to control embryos (n = 3–5 embryos per group). t test. *p < 0.05.

(B) Coronal sections of the neocortex of E12.5 control and *Robo1/2* mutant embryos showing expression of *Hes1*, *Dll1*, and *Notch1* mRNA.

(C) Experimental paradigm used for rescue experiments.

(D–E′) Coronal sections through the cortex of E12.5 + 1DIV *Robo1/2* mutant embryos showing GFP and Tbr2 stains after electroporation with *Gfp* or *Gfp + Hes1*.

Images are full stacks of confocal planes. Arrows and arrowheads point to Tbr2+ and Tbr2– cells, respectively, as assessed from individual confocal plane images.

(F) Quantification of the fraction of Tbr2+ cells present among the Gfp electroporated population. Tbr2+/Gfp+ cell ratio, *Gfp*: 39.2 ± 5.6%, n = 628 cells from three different animals; *Gfp + Hes1*: 4.3 ± 1.3%, n = 1035 cells from three different animals. Mean ± SEM; χ^2-test, ***p < 0.001.

(G) Experimental paradigm used for RNAi experiments.

(H–I′) Coronal sections through the cortex of E14.5 wild-type embryos showing Gfp and Tbr2 stains after electroporation with *Gfp* or *Gfp + Hes1* siRNA. Images are full stacks of confocal planes. Arrows and arrowheads point to Tbr2+ and Tbr2– cells, respectively, as assessed from individual confocal plane images.

(J) Quantification of the fraction of Tbr2+ cells present among the Gfp electroporated population. Tbr2+/Gfp+ cell ratio, *Gfp*: 57.3 ± 0.6%, n = 2354 cells from three different animals; *Gfp + Hes1*: 64.1 ± 1.1%, n = 1949 cells from four different animals. Mean ± SEM; χ^2-test, ***p < 0.001.

Scale bar equals 100 μm (B), 25 μm (D–E′), and 15 μm (H–I′). See also Figure S8.
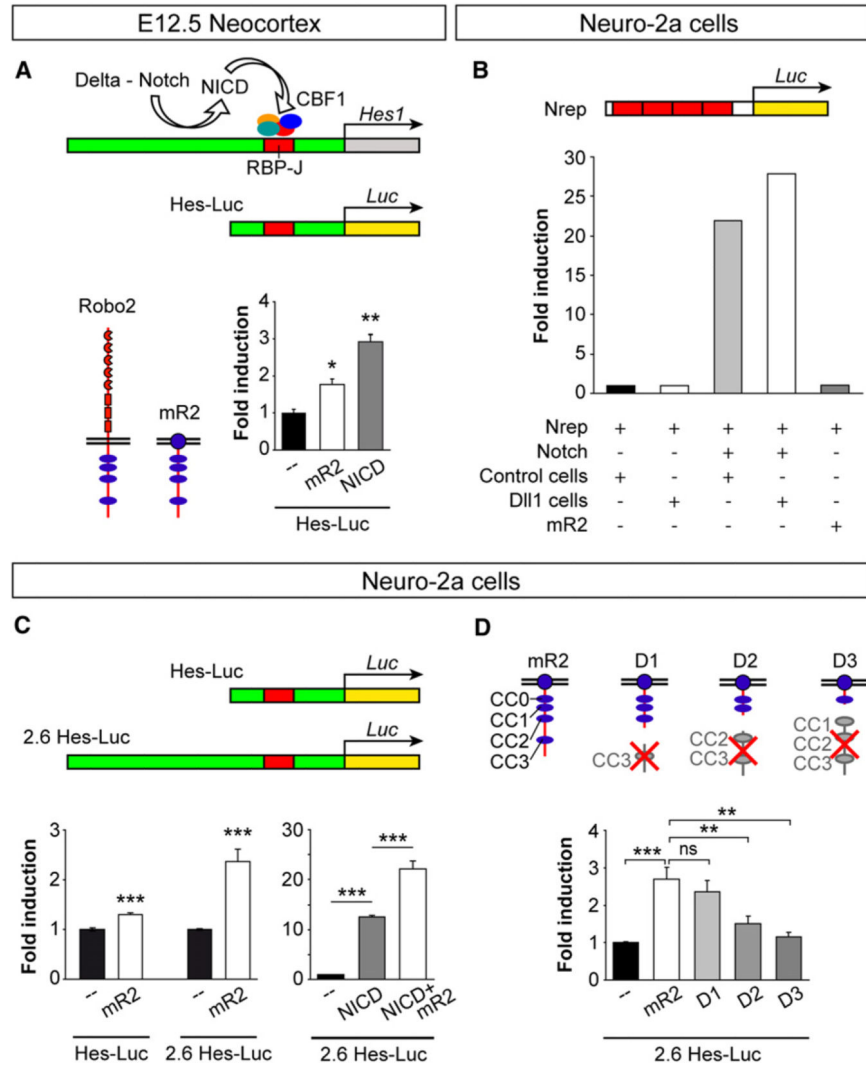
Figure 8. Robo Signaling Drives *Hes1* Transcription

(A) In the developing brain, delta-mediated processing of Notch releases NICD, which interacts with a transcription factor complex that includes CBF1 to activate *Hes1* transcription through RBP-J consensus sequences. The Hes-Luc construct tested contains an RBP-J sequence. Schemas depict the basic structure of full-length Robo2 and the myristoylated version of *Robo2 (mR2)*. The histogram shows fold induction of luciferase (*Luc*) activity from the *Hes-Luc* construct in E12.5 cortical primary cultures after transfection with mR2 or NICD. Mean ± SEM; t test, *p < 0.05; **p < 0.01.

(B) *Hes1* transcription is not activated in Neuro-2a cells upon transstimulation of the Notch pathway with delta. Activation of *Hes1* transcription was assayed with a Notch reporter construct (*Nrep*) containing four RBP-J repeats.

(C) Two different *Hes-Luc* constructs were used with Neuro-2a cells: Hes-Luc and 2.6 Hes-Luc; the latter includes a long 5 ft region. The graphs show fold induction of Hes-Luc and 2.6 Hes-Luc lucif-erase activities after transfection of Neuro-2a cells with mR2, NICD, or NICD+mR2. Mean ± SEM; t test, ***p < 0.001.

(D) Structure of *mR2* and three truncated forms (*D1*, *D2*, and *D3*) and fold induction of 2.6 Hes-Luc luciferase activity in Neuro-2a cells. Statistical significance indicated for *mR2* is with respect to basal activity; all others relate to *mR2*. In addition, *D2* values, but not *D3*, were significantly different than basal values. Mean ± SEM; t test, **p < 0.01; ***p < 0.001.
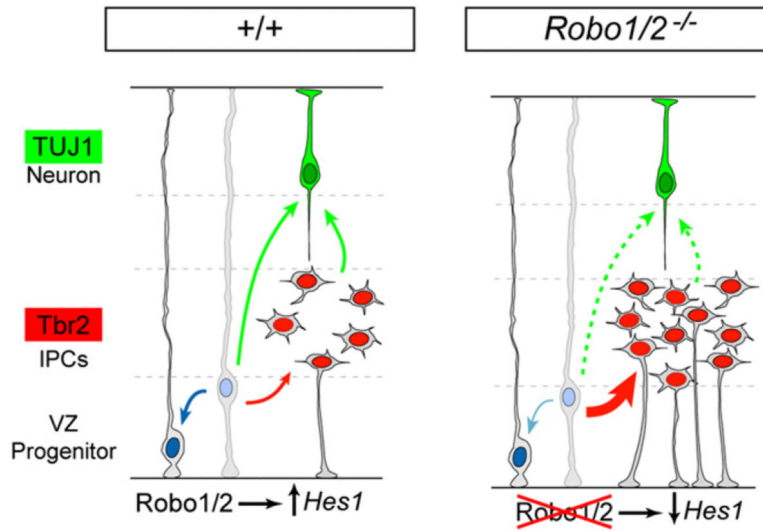
Figure 9. A Model of the Function of Robo Signaling on the Dynamics of Telencephalic Progenitors

In normal development (+/+), Robo signaling drives *Hes1* transcription in neocortical VZ progenitors, which contributes to maintain the balance between VZ progenitor self-renewal (blue arrow), generation of Tbr2+ IPCs (red arrow), and generation of TUJ1+ neurons (green arrows). In the absence of Robo receptors (*Robo1/2⁻/⁻*), *Hes1* mRNA levels decrease and the dynamics of VZ progenitors are unbalanced, favoring the generation of IPCs over self-renewal. For unknown reasons, a large proportion of *Robo1/2* mutant IPCs retain a ventricle-contacting apical process and stall before entering into mitosis, which indirectly prevents the premature overproduction of neurons in *Robo1/2* mutants.